TITLE:

Evaluation of transporter-mediated hepatobiliary transport of newly developed ¹F-labeled pitavastatin derivative, PTV-F1, in rats by PET imaging

AUTHOR(S):

Kimura, Hiroyuki; Yagi, Yusuke; Mikamo, Mutsumi; Kazuya, Maeda; Kagawa, Shinya; Arimitsu, Kenji; Higashi, Tatsuya; ... Togashi, Kaori; Kusuhara, Hiroyuki; Saji, Hideo

京都大学学術情報リポジトリ

KURENAI

Kyoto University Research Information Repository

Evaluation of Transporter-Mediated Hepatobiliary Transport of Newly Developed ^{18}F-labeled Pitavastatin Derivative, PTV-F1, in Rats by PET Imaging

Hiroyuki Kimura[#][*][1,2], Yusuke Yagi[#][1,2], Mutsumi Mikamo[1], Kazuya Maeda[3], Shinya Kagawa[4], Kenji Arimitsu[1,2], Tatsuya Higashi[4,5], Ryuichi Nishii[4,5], Masahiro Ono[1], Yuji Nakamoto[6], Kaori Togashi[6], Hiroyuki Kusuhara[3] and Hideo Saji[*][1]

[1] Department of Patho-Functional Bioanalysis, Graduate School of Pharmaceutical Sciences, Kyoto University, Kyoto, Japan

[2] Department of Analytical and Bioinorganic Chemistry, Kyoto Pharmaceutical University, Kyoto, Japan

[3] Laboratory of Molecular Pharmacokinetics, Graduate School of Pharmaceutical Sciences, The University of Tokyo, Tokyo, Japan

[4] Shiga Medical Center Research Institute, Moriyama, Japan

[5] Department of Molecular Imaging and Theranostics, National Institute of Radiological Sciences (NIRS), National Institutes for Quantum and Radiological Science and Technology (QST), Chiba, Japan

[6] Department of Diagnostic Imaging and Nuclear Medicine, Kyoto University Graduate School of Medicine, Kyoto Japan

[#] These authors contributed equally to this work.

Corresponding Author:

Hiroyuki Kimura, PhD and Hideo Saji, PhD

Department of Patho-Functional Bioanalysis, Graduate School of Pharmaceutical

Sciences, Kyoto University; 46-29 Yoshida Shimoadachi-cho, Sakyo-ku, Kyoto

606-8501, Japan

Tel: +81-75-753-4556, Fax: +81-75-753-4568

E-mail: hkimura@mb.kyoto-phu.ac.jp, hsaji@pharm.kyoto-u.ac.jp

Abbreviations

BCRP: breast cancer resistance protein, KO: knockout, MRP2: multidrug resistance-associated protein 2, OATP: organic anion transporting polypeptide, %ID: percentage of injected dose, PET: positron emission tomography, P-gp: P-glycoprotein, ROI: region of interest, TLC: thin-layer chromatography

・ **Table of contents/Abstract Graphic**
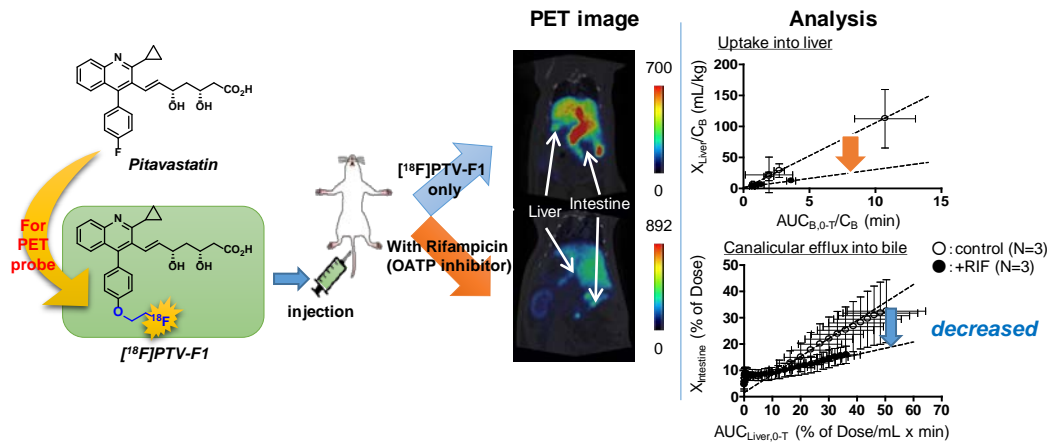
Abstract

Quantitative evaluations of the functions of uptake and efflux transporters directly in vivo is desired to understand an efficient hepatobiliary transport of substrate drugs. Pitavastatin is a substrate of organic anion transporting polypeptides (OATPs) and canalicular efflux transporters; thus, it can be a suitable probe for positron-emission tomography (PET) imaging of hepatic transporter functions. To characterize the performance of [^{18}F]PTV-F1, an analogue of pitavastatin, we investigated the impact of rifampicin (a typical OATP inhibitor) coadministration or Bcrp (breast cancer resistance protein) knockout on [^{18}F]PTV-F1 hepatic uptake and efflux in rats by PET imaging. After intravenous administration, [^{18}F]PTV-F1 selectively accumulated in the liver, and the radioactivity detected in plasma, liver, and bile mainly derived from the parent PTV-F1 during the PET study (~40 min). Coadministration of rifampicin largely decreased the hepatic uptake of [^{18}F]PTV-F1 by 73%. Because of its lower clearance in rats, [^{18}F]PTV-F1 is more sensitive for monitoring changes in hepatic OATP1B function that other previously reported OATP1B PET probes. Rifampicin coadministration also significantly decreased the biliary excretion of radioactivity by 65%. Bcrp knockout did not show a significant impact on its biliary excretion. [^{18}F]PTV-F1 enables quantitative analysis of the hepatobiliary transport system for organic anions.

Keywords

organic anion transporting polypeptide (OATP), positron emission tomography

(PET), fluorine-18, pitavastatin, breast cancer resistance protein (BCRP),

rifampicin, hepatobiliary transport

Introduction

Characterization of the hepatobiliary transport of drugs is a key element for understanding the pathways involved in drug elimination from the body. Various uptake and efflux transporters are coordinately involved in the hepatobiliary transport of drugs in humans[1, 2]. The organic anion transporting polypeptides (OATPs) 1B1 and 1B3 are responsible for the hepatic uptake of anionic drugs, such as 3-hydroxy-3-methylglutaryl-coenzyme A (HMG-CoA) reductase inhibitors (statins). On the canalicular side, P-glycoprotein (P-gp), multidrug resistance-associated protein 2 (MRP2) and breast cancer resistance protein (BCRP) are considered to be important for the efflux of drugs and their metabolites into the bile. Altered functions of these transporters, caused by drug–drug interactions and genetic polymorphisms of specific transporter isoforms, result not only in changes of blood–drug concentrations, but also intrahepatic drug concentrations. According to the extended clearance concept, if the rate-limiting step of intrinsic hepatic clearance of a drug is hepatic uptake, it is possible that the decreased function of canalicular efflux transporters does not affect the blood–drug concentration, but dramatically increases the hepatic concentration[1]. Thus, methods to quantify the intrinsic hepatobiliary transport clearance of each drug particularly with regard to the liver concentration in humans are needed for deep understanding of the factors causing interindividual differences in the canalicular efflux process.

Positron emission tomography (PET) is one of the powerful, noninvasive approaches for molecular imaging in living systems. The high sensitivity and quantitative property of PET make it a useful tool for estimating the in vivo

7

functions of transporters over time using appropriate radiotracers. To directly characterize the hepatobiliary transport systems for organic anions in vivo, several PET probes such as [11C]15R-TIC [3, 4], [11C]dehydropravastatin [5, 6], [11C]telmisartan[7] and [11C]rosuvastatin[8] have been used to elucidate the impact of OATP1Bs-mediated drug interaction with rifampicin and dose-dependent nonlinear pharmacokinetics of drugs in rodents and humans[4]. One important feature of PET probes for the quantification of transport functions is that the PET probes themselves must not undergo extensive metabolism. Otherwise, the pharmacokinetic parameters determined represent a complex of intrinsic parameters for metabolism and membrane transport. 15R-TIC forms at least three metabolites[4] and a substantial amount of telmisartan is glucuronidated[7]; thus, the interpretation of their canalicular efflux as measured by radioactivity is difficult.

Pitavastatin was mainly cleared from the liver where OATP1B1 and OATP1B3 play pivotal roles in its uptake[9]. As for biliary excretion of pitavastatin, Bcrp is the most important transporter in mice[10], whereas Mrp2 is not involved in this process in rats because canalicular efflux clearance of pitavastatin did not change in Mrp2-deficient rats[10] (Eisai hyperbilirubinemic rats), which is different from pravastatin and rosuvastatin[11, 12]. Thus, pitavastatin is expected to have a unique pharmacokinetic character. Moreover, unlike other statins, pitavastatin has fluorine group in its structure, the radioisotope of which ([18F]) has a much longer half-life (109.7 min) than most of the other positron emitting radionuclides commonly incorporated into pharmaceutical agents, such as [11C] (20 min), [13N] (10 min) and [15O] (2 min). The incorporation of [18F] can also be much easier to achieve

than the incorporation of other positron emitting radionuclides with longer half-lives such as ^{124}I (4.2 days) and ^{89}Zr (78.4 h). All previously developed PET probes used to examine hepatobiliary transport were labeled with ^{11}C and the time constraints for handling these compounds need to be considered. We first tried to develop ^{18}F-pitavastatin[13], however, its synthesis was a big challenge (i.e., many steps, and handling of volatile radioactive intermediates); therefore, we designed a PET probe of the pitavastatin derivative, [^{18}F]PTV-F1[14] (Fig. 1). Uptake clearances of PTV-F1 in OATP1B1- and OATP1B3-expressing HEK293 cells were almost the same as those of pitavastatin, and that metabolism of both PTV-F1 and pitavastatin was not detected within 10 min after incubation with human liver microsomes[14]. Thus, the pharmacokinetic property of PTV-F1 is expected to be similar to that of pitavastatin.

The current study intends to characterize the hepatobiliary transport of [^{18}F]PTV-F1 in rats by PET imaging when rifampicin, a typical OATP1Bs inhibitor, was coadministered or Bcrp KO rats was used.

Materials and Methods

Materials

All reagents and solvents were commercially available from Wako Pure Chemical Industries (Tokyo, Japan), Nacalai Tesque (Kyoto, Japan), Merck (Darmstadt, Germany), and Sigma Aldrich (St. Louis, MO, USA), and used as received without further purification. [^{18}F]PTV-F1 was synthesized as previously reported[14]. The identity and concentration of [^{18}F]PTV-F1 were assessed by high-performance liquid chromatography using a Shimadzu system (a LC-10AT pump with a SPD-10A UV detector, σ = 220, 254 nm; Shimadzu, Kyoto, Japan) with a Cosmosil 5C18-ARII column (4.6 × 150 mm and 10 × 250 mm; Nacalai Tesque) and a radioisotope detector. The chemical structure of [^{18}F]PTV-F1 is shown in Figure 1. The radiochemical purity was >95%, and the molar radioactivity was >10.0 GBq/μmol at the time of injection. The purified fraction was evaporated and reconstituted with saline[14].

Animals

Male Sprague Dawley (SD) rats weighing 222–333 g (8–10 weeks old) were purchased from Japan SLC, Inc. (Shizuoka, Japan). Breast cancer resistance protein (Bcrp) gene KO rats (Male, SD-Abcg2^{tm1sage}) weighing 198–252 g (8–10 weeks old) were purchased from Sigma Sage Laboratories (St. Louis, MO, USA). All animals were kept in a temperature- and light-controlled environment with standard food, and tap water was provided ad libitum. The Kyoto University Animal Care Committee approved all animal procedures.

PET scans

All PET and computed tomography (CT) scans were performed using a FX-3300 (Gamma Medica, Salem, NH, USA) designed for laboratory animals. This PET scanner has a spatial resolution of <1 mm in full width at half-maximal (FWHM) at the center of the view at 100 mm in diameter and an axial extent of 110 mm in length. PET experiments with [^{18}F]PTV-F1, either alone or with coadministered rifampicin, were performed in control SD or Bcrp KO rats. Rats were anesthetized and maintained under anesthesia with 1.5% isoflurane, and the femoral artery was cannulated with polyethylene tubing for blood collection. At the start of the emission scan, [^{18}F]PTV-F1 was administered as a single bolus via the tail vein at doses of 8.90 ± 1.44 MBq (n = 11). All PET acquisitions were performed in dynamic scan mode for 60 min.

For estimating the transport function of OATP1Bs in the liver, rifampicin, a typical inhibitor of OATP1Bs, was intravenously infused at a rate of 1.5 μmol/min/kg for at least 90 min before the administration of [^{18}F]PTV-F1, and a constant infusion rate was then kept until the end of the PET scan. Arterial blood was sampled via the cannulated femoral artery 11 times within 30 min at the following time points: 10, 20, 30, 40, and 50 s and 1, 2, 5, 10, 20, and 30 min after bolus administration of [^{18}F]PTV-F1. The volume of blood sampled at each time point was about 10 μL, and the total blood volume sampled from one rat did not exceed 1.6 mL, which is about 10% of the total circulating blood volume. Blood radioactivity levels were measured using a μFmPC system (Shimadzu). Radioactivity in each measured sample was corrected for decay. After finishing

11

the PET scan, CT scans were performed with the following conditions: tube voltage, 60 kV; tube current, 310 μA. Anesthesia was maintained at 1.5% isoflurane before euthanasia, using an injection of sodium pentobarbital.

Analysis of PET data

PET images were reconstructed by Fourier rebinning and standard 3D-ordered-subsets expectation maximization. Regions of interest (ROIs) representing the liver were delineated using the Pmod program (v. 3.3; PMOD Technologies, Zurich, Switzerland). All ROIs were combined and transformed to volumetric regions of interest. The time-radioactivity curve for liver was constructed by normalizing decay-corrected time-radioactivity measurements to the injected dose (% dose) of [^{18}F]PTV-F1.

Biodistribution of radioactivity after [^{18}F]PTV-F1 administration

A saline solution of [^{18}F]PTV-F1 was injected into rats through the tail vein. Animals were sacrificed at a designated time (2, 5, 10, 15, 30, and 60 min after injection). Blood, heart, lung, liver, spleen, pancreas, stomach, intestine, kidney, bone, and whole-brain samples were removed quickly. The radioactivity present in these tissues was measured using a 1480 WIZARD 3 automatic gamma counter (PerkinElmer Co.,Ltd.), and the results were expressed as the percentage of the injected dose (%ID/g). All radioactivity measurements were corrected for decay.

Analysis of metabolites in blood, bile, and liver using thin-layer chromatography (TLC)

Metabolite analysis was carried out as described previously[4]. After the femoral artery and the bile duct in SD rat were cannulated, [^{18}F]PTV-F1 was injected via the tail vein at doses of 41.1 MBq. Arterial blood samples were collected at 1, 2, 5, 10, 20, and 40 min after injection. Bile samples were collected at 0–5, 5–10, 10–25, and 25–40 min after injection. To sample liver tissue, blood flow was terminated by transection of the abdominal aorta and vein at 10, 20, and 40 min after injection, and the liver was quickly removed and homogenized. Blood, bile, and liver samples were deproteinized by precipitation with acetonitrile. After centrifugation (12000 rpm, 2 min, 0 °C), the supernatants were applied to RP-18 TLC plates (Merck KGaA, Darmstadt, Germany).

Plates were developed at room temperature with acetonitrile/water/acetic acid (50:50:0.75) as a mobile phase. After migration, plates were dried and exposed to BAS SR2040 imaging plates (Fuji Film, Tokyo, Japan) for 90–360 min. The distribution of radioactivity on the imaging plates was determined with digital PSL autoradiography using a Fuji BAS-5000 analyzer, and the data were analyzed using the MultiGauge image analysis program (Fuji Film). Rf value was determined PTV-F1 and a lactone form of PTV-F1 which was synthesized[14].

Kinetic analyses of PET data to determine the clearance of radioactivity

The initial uptake clearance of the radioactivity in the liver (CL$_{uptake,liver}$) was calculated by integration plot analyses using the initial linear portion of the curves

13

after [^{18}F]PTV-F1 administration (0.5–2 min). The CL$_{uptake,liver}$ of [^{18}F]PTV-F1 was estimated based on the following equation:

$$\frac{X_{t,liver}}{C_{t,blood}} = CL_{uptake,liver} \times \frac{AUC_{0-t,blood}}{C_{t,blood}} + V_{E,liver}, \tag{1}$$

where X$_{t,liver}$, C$_{t,blood}$, and AUC$_{0-t,blood}$ represent the amount of radioactivity in the liver at time t, the blood concentration of radioactivity at time t, and the area under the blood concentration–time curve from time 0 to time t, respectively. For the estimation of AUC$_{0-t,blood}$, the blood concentration–time curve of the radioactivity was fitted to the two-exponential equation (C$_{B,t}$ = Ae$^{-\alpha t}$ + Be$^{-\beta t}$) to optimize parameters (α, β, A, B). Then, AUC$_{0-t,blood}$ was calculated using the following equation:

$$AUC_{0-t,blood} = \frac{A}{\alpha} \cdot (1 - e^{-\alpha t}) + \frac{B}{\beta} \cdot \left(1 - e^{-\beta t}\right) \tag{2}$$

CL$_{uptake,liver}$ was obtained from the initial slope of the plot of X$_{t,liver}$/C$_{t,blood}$ versus AUC$_{0-t,blood}$/C$_{t,blood}$. V$_{E,liver}$ represents the initial distribution volume in the liver at time 0, which was calculated from the y-intercept of the integration plot.

The canalicular efflux clearance of the radioactivity in the liver (CL$_{int,bile}$) was calculated by integration plot analyses using the later phase of the time–radioactivity curves that maintained the linearity of the integration plot (4–13 min) after [^{18}F]PTV-F1 administration. CL$_{int,bile}$ of radioactivity was estimated based on the following equation:

$$X_{t,bile} = CL_{int,bile} \times AUC_{0-t,liver} + X_E, \tag{3}$$

where X$_{t,bile}$ and AUC$_{0-t,liver}$ represent the estimated radioactivity excreted into the bile as the sum of the radioactivity in the gallblader and bile duct and "intestine" (the radioactivity in both intestinal tissue and luminal content) at time t, which

14

corresponds to the putative biliary-excreted radioactivity, and the area under the hepatic concentration–time curve from time 0 to time t, respectively. Although we did not experimentally confirm the relative contribution of biliary excretion and intestinal secretion to the overall accumulation of the radioactivity in the intestine in rats, we assumed that the radioactivity in the intestine mostly came from its biliary excretion for the estimation of $CL_{int,bile}$ since previous report indicated that 93% of initially-administered radioactivity was collected in the bile for 96 hours after intravenous administration of $[^{14}C]$pitavastatin in bile duct-cannulated male rats [15]. $AUC_{0-t,liver}$ was calculated based on the linear trapezoidal rule. $CL_{int,bile}$ was obtained from the initial slope of the plot of $X_{t,bile}$ versus $AUC_{0-t,liver}$. X_E represents the initial distribution volume in the bile at time 0, which was calculated from the y-intercept of the integration plot.

Statistical analysis

Student's two-tailed t-test was used to identify significant differences in the kinetic parameters between control rats, and rifampicin-treated rats or Bcrp KO rats. Statistical significance was set at $p < 0.05$.

Results

Biodistribution of radioactivity in the abdominal region after intravenous administration of [^{18}F]PTV-F1

The tissue distribution of radioactivity in normal SD rats over time after administration of [^{18}F]PTV-F1 is shown in Fig. 2 and Supplemental Table 1. In normal SD rats without any concomitantly-administered drugs, the radioactivity was predominantly present in the liver in the early phase (32.9 ± 2.5%ID at 2 min) and gradually moved into the intestine in the later phase (61.9 ± 8.4%ID at 60 min), which suggests that a major part of the administered [^{18}F]PTV-F1 was subsequently excreted into the bile. Radioactivity was also detected in the kidney at early time points after administration of [^{18}F]PTV-F1, but rapidly disappeared within 10 min. However, no clear distribution of radioactivity to other tested organs was observed. In the presence of rifampicin, as shown in Fig. 2, the amount of the radioactivity accumulated in the liver and intestine was clearly less than that in the absence of rifampicin, suggesting that hepatobiliary transport of [^{18}F]PTV-F1 was modified by coadministration of rifampicin, an OATP inhibitor.

16

Radiometabolite analysis of [¹⁸F]PTV-F1 in blood, liver, and bile by TLC autoradiography

In normal SD rats, the fraction of radioactivity from parent PTV-F1 and its metabolites in blood, liver, and bile at the designated time points after [¹⁸F]PTV-F1 administration was estimated by TLC autoradiography (Fig. 3, Supplemental Table 2). Analysis of the TLC autoradiograms showed that virtually no metabolites were detectable in the blood. In the liver extracts, one metabolite (M1) was barely detectable after administration of [¹⁸F]PTV-F1, but almost all radioactivity derived from intact [¹⁸F]PTV-F1 (95.0% at 40 min, Supplemental Table 2). As for bile extracts, though a lactone form of PTV-F1[14] and two metabolites (M1 and M2) were identified, 85.6% of the radioactivity was derived from intact [¹⁸F]PTV-F1 at 40 min after [¹⁸F]PTV-F1 administration (Supplemental Table 2).

Effect of rifampicin coadministration on the time courses of radioactivity in blood, liver, and intestine after intravenous bolus administration of [^{18}F]PTV-F1 in rats

Radioactivity in blood samples was eliminated in a biphasic manner in both control and rifampicin-treated rats (Fig. 4A). However, when rifampicin was coadministered, elimination of the radioactivity was delayed and its blood AUC$_{0-30}$, normalized by [^{18}F]PTV-F1 dose, was 3.4-fold larger in rifampicin-treated rats compared with control SD rats (control (n = 8): 21.1 ± 9.4 [% of dose/mL*min], + rifampicin (n = 3): 71.1 ± 23.6 [% of dose/mL*min]). In the liver of control rats, a maximum of 33.6 ± 5.0% of the injected dose was distributed at 4 min after [^{18}F]PTV-F1 administration, and the radioactivity decreased until the end of the PET scan (Fig. 4B). In rifampicin-treated rats, however, maximum radioactivity in the liver (20.6 ± 3.1% at 5 min) was decreased to 61% of that in control rats and liver-associated radioactivity decreased much more slowly over time, especially in the earlier phase (5–15 min). As for the radioactivity in the intestine, it increased over time with some time delay (~3 min) and reached 38.9 ± 14.7% of the injected dose at 30 min in control rats, whereas in rifampicin-treated rats, the maximum radioactivity in the intestine at 30 min (21.1 ± 3.5%) was dramatically reduced to 54% of that in control rats (Fig. 4C).

Effect of rifampicin coadministration on the hepatic uptake and canalicular efflux clearance of [^{18}F]PTV-F1

The integration plots for hepatic uptake clearance and canalicular efflux clearance are shown in Fig. 5 and their kinetic parameters are summarized in Table 1. Linearity of the plot was maintained for a short time period between 0.5–2 min for liver uptake. In rifampicin-treated rats, $CL_{uptake,liver}$ was significantly decreased to 27% of the control values. Regarding the canalicular efflux, the linear range of the plot was reached between 4-13 min, because of the time lag required for the radioactivity to reach the liver. The $CL_{int,bile}$ of the radioactivity in rifampicin-treated rats was significantly decreased to 35% of the control values.

Effect of Bcrp KO on the time courses of the radioactivity in blood, liver, and intestine after intravenous bolus administration of [^{18}F]PTV-F1 in rats

Radioactivity in blood samples was also eliminated in a biphasic manner in Bcrp KO rats (Fig. 6A). The elimination of radioactivity was delayed at the later phase, and its blood AUC_{0-30}, normalized by [^{18}F]PTV-F1 dose, was 2.1-fold larger in Bcrp KO rats compared with control SD rats (Bcrp KO rats (n = 3): 43.7 ± 8.6 [% of dose/mL*min]). In the liver of Bcrp KO rats, maximum radioactivity (39.7 ± 6.4% of dose at 4 min) was slightly increased to 118% of that in control rats. Overall radioactivity in the liver tended to be higher in Bcrp KO mice than in control SD rats, although that difference did not reach statistical significance. As for the radioactivity in the intestine, its time course in Bcrp KO rats was not different from that in control rats.

Effect of Bcrp gene KO on the hepatic uptake and canalicular efflux clearance of [^{18}F]PTV-F1

The integration plots for hepatic uptake clearance and canalicular efflux clearance are shown in Fig. 7, and their kinetic parameters are summarized in Table 1. $CL_{uptake,liver}$ was not significantly different between control and Bcrp KO rats. Regarding canalicular efflux, the $CL_{int,bile}$ of the radioactivity showed a slight, but not statistically significant, decrease by Bcrp KO.

Discussion

In the present study, kinetic analyses of the hepatobiliary transport of [^{18}F]PTV-F1 in rats were carried out using PET imaging as a feasibility study. As expected, coadministration of rifampicin, a typical OATP inhibitor, reduced both hepatic uptake and canalicular efflux clearance, confirming that membrane transport of [^{18}F]PTV-F1 was mainly mediated by transporters in the rat liver. Regarding [^{18}F]PTV-F1's canalicular efflux, contrary to our expectations from the previous pharmacokinetic analyses of pitavastatin in mice [10], Bcrp does not have a major impact on it in rats.

After intravenous administration of [^{18}F]PTV-F1 in control rats, radioactivity accumulated primarily in the liver and, to a lesser extent, in the kidney (Fig. 2, Supplemental Table 1). Previous whole-body autoradiography of rats after intravenous administration of [^{14}C]pitavastatin indicated that radioactivity mainly accumulated in the liver and kidney at 2.5 min, while high levels of radioactivity were found in the liver and intestine at 60 min[15]. This is consistent with the tissue distribution pattern of [^{18}F]PTV-F1 (Supplemental Table 1). The radioactivity in the liver of control SD rats at 2, 5, 10, 15, and 30 min, obtained from PET imaging, was estimated to be 31 ± 5%, 33 ± 5%, 26 ± 6%, 20 ± 7%, and 13 ± 11% (mean ± SD) of the injected dose, respectively (Fig. 4). These data are very similar to the data obtained from the separate conventional biodistribution study (Supplemental Table 1), suggesting that ROIs of liver were delineated properly.

The fraction of unchanged PTV-F1 in the total radioactivity in blood, liver and bile after intravenous administration of [^{18}F]PTV-F1 was evaluated using TLC.

22

Metabolites were virtually untraceable in the blood, while very low amounts of one metabolite (M1) were detected in the liver, and lactone form of PTV-F1, as well as two other metabolites (M1, M2), was detected in the bile. Our analyses indicated that most of the radioactivity was derived from parent PTV-F1 and that kinetic parameters estimated from this PET study should correctly reflect the hepatobiliary transport of PTV-F1 itself. In the case of pitavastatin, a previous study showed that 84%, 95%, and 85% of the total radioactivity was derived from parent pitavastatin in plasma, liver, and bile at 60 min after intravenous administration of [14C]pitavastatin, respectively[15]. These results confirm that PTV-F1, as well as pitavastatin, can be categorized as nonmetabolized types of statin, at least in rats.

Although we have not measured the cumulative radioactivity in the feces and urine for a long time after intravenous administration of [18F]PTV-F1 in rats, considering the similar time profiles of the tissue distribution including little accumulation in the kidney of PTV-F1 and pitavastatin[15], we consider that PTV-F1 is mostly excreted into bile in an unchanged form.

When rifampicin was coadministered, blood concentration of the radioactivity became significantly higher even at 2 min after [18F]PTV-F1 administration compared with control rats, and radioactivity in the liver and intestine was significantly lower. In the current study, the same protocol of rifampicin administration (constant infusion of 1.5 μmol/min/kg for >90 min) was applied as that used in the previous PET studies with [11C]dehydropravastatin and [11C]telmisartan[5, 7]. Under this condition, unbound blood concentration of rifampicin was 11–13 μM at steady state in rats, which is high enough to potently

inhibit rat Oatp1a4 (K_i = 1.46 μM) and Oatp1b2 (K_i = 0.79 μM) and to partly inhibit rat Oatp1a1 (K_i = 18.2 μM) [16, 17]. Then, hepatic uptake clearance ($CL_{uptake,liver}$) was determined using integration plot analyses. $CL_{uptake,liver}$ of [18F]PTV-F1 was decreased to 27% of the control by coadministration of rifampicin. Compared with our results, the degree of decrease in $CL_{uptake,liver}$ of [11C]telmisartan (65% of control) and [11C]dehydropravastatin (69% of control) was relatively smaller[5, 7]. This can be explained partly because $CL_{uptake,liver}$ values of [11C]telmisartan and [11C]dehydropravastatin were almost equal to the hepatic blood flow rate, while that of [18F]PTV-F1 was ca. one-sixth of the hepatic blood flow rate. Thus, compared with other reported probes, [18F]PTV-F1 has a higher sensitivity for detecting the inhibitory effect of drugs on hepatic OATP1B transporters. In vitro uptake clearance of pitavastatin into rat hepatocytes was reported to be 121–444 μL/min/mg protein[18, 19], which corresponds to a $CL_{uptake,liver}$ of 10.4–26.1 mL/min/kg, assuming a well-stirred model with physiological scaling factors[19] (1.2 $\times$ 10^8 cells/g liver, 41.2g liver/kg; f_B of pitavastatin in rats = 0.021). Thus, hepatic uptake clearance of [18F]PTV-F1 is almost comparable to that of pitavastatin in rats. On the other hand, initial distribution volume in the liver was significantly changed in the presence of rifampicin (Table. 1). Since the value of Y-intercept in the integration plot is small and largely depends on the range of data used for the determination of initial slope by line fitting and individual data are very variable, we do not want to go into its interpretation further.

Canalicular efflux clearance ($CL_{int,bile}$) of [18F]PTV-F1 was also decreased to 35% of control by rifampicin coadministration as reported previously with

24

[^{11}C]dehydropravastatin (41% of control)[7].   Though exact mechanism of the canalicular efflux of dehydropravastatin has not been clarified, genetic deficiency of Mrp2 almost impaired the biliary excretion of pravastatin in rats[11], thus decreased excretion of dehydropravastatin by rifampicin was thought to be mainly caused by the inhibition of Mrp2.   However, our previous study indicated that canalicular efflux of pitavastatin was not mediated by Mrp2 in rats[10]. According to the University of Washington Metabolism and Transport Drug Interaction Database, the geometric mean values of reported half-maximal inhibitory concentration of rifampicin for human P-gp, MRP2, and BCRP are 53.6 μM (range: 4.3–279 μM), 33.9 μM (range: 7.9–144 μM), and 47.6 μM (range: 14–461 μM), respectively. Considering that rifampicin actively accumulates in the liver and that Mrp2-mediated transport of the radioactivity of PET ligands was decreased by rifampicin[5, 7], all these transporters are possibly inhibited by rifampicin coadministration to a similar extent. In mice, pitavastatin was excreted into the bile mainly via Bcrp[10]. Then, the relative contribution of Bcrp to the overall biliary excretion of [^{18}F]PTV-F1 was investigated with Bcrp KO rats. Surprisingly, canalicular efflux clearance of [^{18}F]PTV-F1 radioactivity was not significantly different between Bcrp KO and control rats.   We have not checked whether PTV-F1 is a substrate of rat Bcrp or not due to the limited availability of PTV-F1 for in vitro transport experiments. Thus, it is possible that pitavastatin and PTV-F1 are recognized by Bcrp differently as substrates. Alternatively, it is possible that each single isoform of efflux transporter did not exclusively dominate the canalicular efflux of [^{18}F]PTV-F1.   Further analyses are needed to rationally

25

explain this phenomenon by comparing the hepatobiliary transport of [18F]PTV-F1 and [18F]pitavastatin, whose synthesis strategy was also recently established[13], in KO rats of each efflux transporter.

In summary, we quantitatively detected changes in the hepatobiliary transport of a novel [18F]-labeled, nonmetabolized type of PET ligand, [18F]PTV-F1, when it is coadministrated with rifampicin, a typical OATP inhibitor in rats. [18F]PTV-F1 is suitable for the sensitive detection of functional changes in OATP transporters due to drug–drug interactions or some other special occasions because hepatic clearance was not limited by hepatic blood flow rate. This pharmacokinetic property is also applicable in humans; thus, it is expected that [18F]PTV-F1 performs similarly in detecting functional changes in OATP1Bs in human PET study. However, canalicular efflux of [18F]PTV-F1-derived radioactivity decreased by rifampicin administration, but Bcrp did not significantly contribute to its canalicular efflux. If the molecular mechanisms of canalicular efflux of PTV-F1 are clarified, it will be used as a novel type of anionic PET probe whose responsible biliary excretion transporter is distinct from MRP2, that is different from the reported PET probes of OATP substrates.

Conflict of Interest

The authors have no conflicts of interest.

Acknowledgements

Author contributions

Wrote Manuscript: Kimura, Yagi, Mikamo, Maeda and Kusuhara

Designed Research: Kimura, Yagi, Maeda, Kusuhara and Saji

Performed Research: Kimura, Yagi, Mikamo, Arimitsu and Kagawa

Analyzed Data: Kimura, Yagi, Mikamo and Maeda

Contributed New Reagents/Analytical Tools: Kimura, Yagi, Mikamo, Arimitsu, Ono, Nishii, Higashi, Nakamoto, Togashi and Saji

References

[1] Yoshida K, Maeda K, Sugiyama Y. Hepatic and intestinal drug transporters: prediction of pharmacokinetic effects caused by drug-drug interactions and genetic polymorphisms. Annu Rev Pharmacol Toxicol 2013;53:581-612.

[2] Zamek-Gliszczynski MJ, Taub ME, Chothe PP, Chu X, Giacomini KM, Kim R B, Ray AS, Stocker SL, Unadkat JD, Wittwer MB, Xia C, Yee SW, Zhang L, Zhang Y. International Transporter C. Transporters in Drug Development: 2018 ITC Recommendations for Transporters of Emerging Clinical Importance. Clin Pharmacol Ther 2018; 104:890-9.

[3] Takashima T, Kitamura S, Wada Y, Tanaka M, Shigihara Y, Ishii H, Ijuin R, Shiomi S, Nakae T, Watanabe Y, Cui Y, Doi H, Suzuki M, Maeda K, Kusuhara H, Sugiyama Y, Watanabe Y. PET imaging-based evaluation of hepatobiliary transport in humans with (15R)-^{11}C-TIC-Me. J Nucl Med 2012;53:741-8.

[4] Takashima T, Nagata H, Nakae T, Cui Y, Wada Y, Kitamura S, Doi H, Suzuki M, Maeda K, Kusuhara H, Sugiyama Y, Watanabe Y. Positron emission tomography studies using (15R)-16-m-[^{11}C]tolyl-17,18,19,20-tetranorisocarbacyclin methyl ester for the evaluation of hepatobiliary transport. J Pharmacol Exp Ther 2010;335:314-23.

[5] Shingaki T, Takashima T, Ijuin R, Zhang X, Onoue T, Katayama Y, Okauchi T, Hayashinaka E, Cui Y, Wada Y, Suzuki M, Maeda K, Kusuhara H, Sugiyama Y, Watanabe Y. Evaluation of Oatp and Mrp2 activities in hepatobiliary excretion using newly developed positron emission tomography tracer [^{11}C]dehydropravastatin in rats. J Pharmacol Exp Ther 2013;347:193-202.

[6] Kaneko K, Tanaka M, Ishii A, Katayama Y, Nakaoka T, Irie S, Kawahata H, Yamanaga T, Wada Y, Miyake T, Toshimoto K, Maeda K, Cui Y, Enomoto M, Kawamura E, Kawada N, Kawabe J, Shiomi S, Kusuhara H, Sugiyama Y, Watanabe Y. A Clinical Quantitative Evaluation of Hepatobiliary Transport of [^{11}C]Dehydropravastatin in Humans Using Positron Emission Tomography. Drug Metab Dispos 2018;46:719-28.

[7] Takashima T, Hashizume Y, Katayama Y, Murai M, Wada Y, Maeda K, Sugiyama Y, Watanabe Y. The involvement of organic anion transporting polypeptide in the hepatic uptake of telmisartan in rats: PET studies with [^{11}C]telmisartan. Mol Pharm 2011;8:1789-98.

[8] He J, Yu Y, Prasad B, Link J, Miyaoka RS, Chen X, Unadkat JD. PET imaging of Oatp-mediated hepatobiliary transport of [^{11}C] rosuvastatin in the rat. Mol Pharm 2014;11:2745-54.

[9] Hirano M, Maeda K, Shitara Y, Sugiyama Y. Contribution of OATP2 (OATP1B1) and OATP8 (OATP1B3) to the hepatic uptake of pitavastatin in humans. J Pharmacol Exp Ther 2004;311:139-46.

[10] Hirano M, Maeda K, Matsushima S, Nozaki Y, Kusuhara H, Sugiyama Y. Involvement of BCRP (ABCG2) in the biliary excretion of pitavastatin. Mol Pharmacol 2005;68:800-7.

[11] Yamazaki M, Kobayashi K, Sugiyama Y. Primary active transport of pravastatin across the liver canalicular membrane in normal and mutant Eisai hyperbilirubinemic rats. Biopharm Drug Dispos 1996;17:607-21.

29

[12] Kitamura S, Maeda K, Wang Y, Sugiyama Y. Involvement of multiple transporters in the hepatobiliary transport of rosuvastatin. Drug Metab Dispos 200;36:2014-23.

[13] Yagi Y, Kimura H, Arimitsu K, Ono M, Maeda K, Kusuhara H, Kajimoto T, Sugiyama Y, Saji H. The synthesis of [18F]pitavastatin as a tracer for hOATP using the Suzuki coupling. Org Biomol Chem 2015;13:1113-21.

[14] Kimura H, Yagi Y, Arimitsu K, Maeda K, Ikejiri K, Takano J, Kusuhara H, Kagawa S, Ono M, Sugiyama Y, Saji H. Radiosynthesis of novel pitavastatin derivative ([18F]PTV-F1) as a tracer for hepatic OATP using a one-pot synthetic procedure. J Labelled Compd Radiopharm 2016;59: 565-75.

[15] Kimata H, Fujino H, Koide T, Yamada Y, Tsunenari Y, Yanagawa Y. Studies on the Metabolic Fate of NK-104, a New Inhibitor of HMG-CoA Reductase (1) : Absorption, Distribution, Metabolism and Excretion in Rats. Drug Metabolism and Pharmacokinetics 1998;13:484-99.

[16] Shitara Y, Sugiyama D, Kusuhara H, Kato Y, Abe T, Meier PJ, Itoh T, Sugiyama Y. Comparative inhibitory effects of different compounds on rat oatpl (slc21a1)- and Oatp2 (Slc21a5)-mediated transport. Pharm Res 2002; 19:147-53.

[17] Lau YY, Okochi H, Huang Y, Benet LZ. Multiple transporters affect the disposition of atorvastatin and its two active hydroxy metabolites: application of in vitro and ex situ systems. J Pharmacol Exp Ther 2006;316:762-71.

[18] Shimada S, Fujino H, Morikawa T, Moriyasu M, Kojima J. Uptake mechanism of pitavastatin, a new inhibitor of HMG-CoA reductase, in rat hepatocytes. Drug Metab Pharmacokinet 2003;18:245-51.

[19] Watanabe T, Kusuhara H, Maeda K, Kanamaru H, Saito Y, Hu Z, Sugiyama Y. Investigation of the rate-determining process in the hepatic elimination of HMG-CoA reductase inhibitors in rats and humans. Drug Metab Dispos 2010;38:215-22.

Figure legends

Figure 1. Chemical structure of [^{18}F]PTV-F1 and pitavastatin

Figure 2. Representative color-coded PET images of rat abdominal region after intravenous administration of [^{18}F]PTV-F1.

Coronal maximum intensity projection PET images of radioactivity in the abdominal region were captured at 2, 5, 10, 20, and 30 min in control (A) and rifampicin-treated (B) rats.

Figure 3. Representative TLC autoradiograms of blood, liver, and bile extracts in rats after intravenous administration of [^{18}F]PTV-F1

Each line represents authentic [^{18}F]PTV-F1 sample (PTV-F1(aus.)), and blood, liver and bile extract samples collected at the designated time points after intravenous administration of [^{18}F]PTV-F1. We have confirmed that the location of the PTV-F1 lactone band is identical to the Rf values of PTV-F1 lactone created by ourselves (Rf = 0.13–0.14).

Figure 4. Time profiles of the radioactivity in the blood (A), liver (B), and intestine (C) after intravenous administration of [^{18}F]PTV-F1 in control and rifampicin-treated rats.

Time profiles of the radioactivity (mean ± SD) in the blood (A), liver (B), and intestine (C) were determined by serial PET images of the abdominal region over a 30-min period after administration of [^{18}F]PTV-F1 in control (open circle; n = 8) and rifampicin-treated (closed circle; n = 3) rats.

32

Figure 5. Integration plots for the determination of hepatic uptake (A) and canalicular efflux (B) after intravenous administration of [^{18}F]PTV-F1 in control and rifampicin-treated rats.

Integration plots were drawn for the hepatic uptake (A) and canalicular efflux (B) in control (open circle; n = 8) and rifampicin-treated (closed circle; n = 3) rats. Each dotted line of the integration plot represents the initial slope of the plots (averaged values). The data represent the mean ± SD.

Figure 6. Time profiles of the radioactivity in the blood (A), liver (B), and intestine (C) after intravenous administration of [^{18}F]PTV-F1 in control and Bcrp KO rats. Time profiles of the radioactivity (mean ± SD) in the blood (A), liver (B), and intestine (C) were determined by serial PET images of the abdominal region over a 30-min period after [^{18}F]PTV-F1 administration in control (open circle; n = 8) and Bcrp KO (closed circle; n = 3) rats.

Figure 7. Integration plots for the determination of hepatic uptake (A) and canalicular efflux (B) after intravenous administration of [^{18}F]PTV-F1 in control and Bcrp KO rats.

Integration plots were drawn for the hepatic uptake (A) and canalicular efflux (B) in control (open circle; n = 8) and rifampicin-treated (closed circle; n = 3) rats. Each dotted line of integration plot represents the initial slope of the plots (averaged values). The data represent the mean ± SD.

Table 1. Effects of rifampicin coadministration and Bcrp KO on the hepatic

uptake clearance, canalicular efflux clearance and initial distribution volume in

the liver at time 0 of the radioactivity in rats after intravenous administration of

[^{18}F]PTV-F1

	$CL_{uptake,liver}$ (mL/min/kg)	V_d (mL/kg)	$CL_{int,bile}$ (mL/min/kg)
Control	10.6 ± 3.6	−0.502 ± 1.461	0.685 ± 0.334
+ Rifampicin	2.87 ± 0.24**	1.86 ± 0.27**	0.237 ± 0.045*
Bcrp-KO	8.20 ± 1.90	0.446 ± 0.216	0.435 ± 0.071

**: $p < 0.01$. *: $p < 0.05$ vs control.

[^{18}F]PTV-F1   pitavastatin

Figure 1.

(A) liver, kidney, intestine — 700 / 0

(B) — 892 / 0

2 min 5 min 10 min 20 min 30 min

Figure 2.

Figure 3.

Figure 4.

(A) Hepatic Uptake

(B) Biliary Excretion

Figure 5.

Figure 6.

(A) Hepatic Uptake

(B) Biliary Excretion

O : control (N=8)
● : Bcrp KO (N=3)

Figure 7.